Draft version July 27, 2016
Preprint typeset using LaTeX style AASTeX6 v. 1.0

arXiv:1607.07732v1 [astro-ph.SR] 26 Jul 2016

HUBBLE SPACE TELESCOPE CONSTRAINTS ON THE WINDS AND ASTROSPHERES OF RED GIANT STARS[1]

Brian E. Wood
Naval Research Laboratory, Space Science Division, Washington, DC 20375, USA; brian.wood@nrl.navy.mil

Hans-Reinhard Müller
Department of Physics and Astronomy, Dartmouth College, Hanover, NH 03755, USA

Graham M. Harper
CASA, University of Colorado, Boulder, CO 80309-0389, USA

[1]Based on observations made with the NASA/ESA Hubble Space Telescope, obtained at the Space Telescope Science Institute, which is operated by the Association of Universities for Research in Astronomy, Inc., under NASA contract NAS 5-26555. These observations are associated with program GO-13462. This paper also presents observations obtained with the Harlan J. Smith Telescope at McDonald Observatory of the University of Texas at Austin.

ABSTRACT

We report on an ultraviolet spectroscopic survey of red giants observed by the *Hubble Space Telescope*, focusing on spectra of the Mg II h & k lines near 2800 Å in order to study stellar chromospheric emission, winds, and astrospheric absorption. We focus on spectral types between K2 III and M5 III, a spectral type range with stars that are noncoronal, but possessing strong, chromospheric winds. We find a very tight relation between Mg II surface flux and photospheric temperature, supporting the notion that all K2-M5 III stars are emitting at a basal flux level. Wind velocities (V_w) are generally found to decrease with spectral type, with V_w decreasing from ~ 40 km s^{-1} at K2 III to ~ 20 km s^{-1} at M5 III. We find two new detections of astrospheric absorption, for σ Pup (K5 III) and γ Eri (M1 III). This absorption signature had previously only been detected for α Tau (K5 III). For the three astrospheric detections the temperature of the wind after the termination shock correlates with V_w, but is lower than predicted by the Rankine-Hugoniot shock jump conditions, consistent with the idea that red giant termination shocks are radiative shocks rather than simple hydrodynamic shocks. A full hydrodynamic simulation of the γ Eri astrosphere is provided to explore this further.

Keywords: stars: chromospheres — stars: late-type — stars: winds, outflow — ultraviolet: stars

1. INTRODUCTION

Ultraviolet and X-ray observations have demonstrated that among main sequence stars stellar coronae are a ubiquitous phenomenon, with coronal emissions being detectable for all stars with spectral types later than A5 V (e.g., Schmitt 1997). This is not the case, however, above the main sequence. For giant stars, F and G type giants are coronal, but this coronal emission either disappears entirely or at least dramatically weakens for K and M type giants. For the K and M giants, the coronae seem to be largely replaced by strong winds ($\dot{M} \sim 10^{-11}$ M$_\odot$ yr^{-1}) at chromospheric temperatures ($T \sim 10^4$ K). The first recognition of the existence of this coronal dividing line among evolved stars between coronal and "windy" stars was by Linsky & Haisch (1979). If attention is limited to giant stars, i.e. luminosity class III stars, the dividing line lies at a spectral type of about K2 III (Haisch et al. 1991). The nature of the transition across this dividing line is a topic of particular interest. Some stars to the right of the dividing line, referred to as "hybrid chromosphere" stars, seem to maintain some level of coronal emission, with γ Dra (K5 III) being perhaps the best-studied luminosity class III example (Ayres et al. 1997). This has led to the proposition that magnetic loops with coronal temperatures still persist beyond the dividing line, but the coronal emissions from these loops are completely or mostly hidden by the dense, thick chromospheres that have developed for such stars, from

which emanate the strong chromospheric winds (Ayres et al. 2003). In order to further investigate the transition from coronae to chromospheric winds, we here present a new survey of red giant stars with spectral types later than K2 III, using UV spectra taken by the *Hubble Space Telescope* (HST).

We are not only interested in the winds of these stars, but also in the interactions of these winds with the interstellar medium (ISM). Ultraviolet spectroscopy from HST has provided the first spectroscopic detections of the wind-ISM interaction regions, or "astrospheres," of many cool stars, including the heliospheric structure surrounding our own Sun. Hydrogen Lyman-α absorption has been observed from the "hydrogen wall" region outside the heliopause (Linsky & Wood 1996), and from the heliotail (Wood et al. 2014a). Hydrogen wall absorption has also been observed around other Sun-like stars, representing the first method by which solar-like coronal winds can be detected around other stars (Wood et al. 2005a, 2014b).

However, we are here interested in the astrospheres of red giant stars. Observations of the Mg II h & k lines near 2800 Å have been used to detect absorption from the astrosphere of α Tau (K5 III) (Robinson et al. 1998; Wood et al. 2007). Models of the α Tau astrosphere were computed using codes designed to study the heliosphere. Analogous to the solar wind, the red giant wind expands radially from the star until it reaches the termination shock (TS), where it is shocked to subsonic speeds. The post-TS wind is slower, hotter, and more dense. It is this post-TS region that provides Mg II column densities sufficiently high to yield the observed Mg II astrospheric absorption.

Due to its high positive stellar radial velocity ($V_{rad} = +54.3$ km s^{-1}), our line of sight towards α Tau is estimated to be at an angle of $\theta \sim 170°$ from the upwind direction of the ISM flow vector in the rest frame of the star. This line of sight is therefore very much through the "astrotail," and this may be essential for detecting the astrospheric absorption. A downwind line of sight provides a much longer path length through the post-TS material than an upwind or sidewind line of sight, leading to much higher column densities through the post-TS material (Wood et al. 2007). Nevertheless, the hydrodynamic models of the α Tau astrosphere were unable to reproduce the observed astrospheric absorption very well, predicting far too little absorption, and placing the absorption farther from the stellar rest frame than observed. The proposed explanation was that the α Tau TS is a radiative shock, with radiative cooling from H Lyman lines yielding further compression and deceleration behind the TS, resulting in a stronger Mg II absorption feature closer to the rest frame of the star, in better agreement with the observed absorption (Wood et al. 2007).

The α Tau observation has long been the only example of a detected red giant astrosphere. Our new HST survey of red giant stars was not only designed to study the red giant winds, but also designed to try to find new detections of astrospheric absorption around such stars.

2. THE HST RED GIANT SURVEY

We are interested in the warm, partially ionized winds and resulting astrospheres of giants with spectral types between K2 III and M5 III. We do not consider stars later than M5, because such giants contain Miras and other long period variables, which have cooler and more massive winds of a different character, and we do not consider giants earlier than K2, which lie on the wrong side of the coronal dividing line mentioned in section 1, exhibiting high-temperature coronal emission instead of strong chromospheric winds (e.g., Haisch et al. 1991). Based on the idea that a downwind line of sight through the astrotail is essential for detecting the Mg II astrospheric absorption signature, all the selected targets have $V_{rad} \geq +40$ km s^{-1}. This choice has the added benefit of shifting the astrospheric absorption and stellar wind absorption away from the expected locations of narrow interstellar Mg II absorption, which can confuse analysis of the line profile.

Table 1 lists properties of the nine red giants that constitute our new red giant survey sample. Within the HST archives, there are high resolution Mg II spectra of four other K2-M5 III stars. These stars are also listed in Table 1, as we will consider their Mg II spectra as well, although only α Tau has the high V_{rad} that we presume to be advantageous for astrospheric detection. The properties listed in Table 1 are spectral type, V band magnitude, V-K color, temperature, radius, distance, radial velocity (V_{rad}), logarithmic Mg II surface flux (F_{MgII}, in ergs cm^{-2} s^{-1} units), stellar wind terminal velocity (V_w), the ISM velocity seen by the star (V_{ISM}), and the orientation of our line of sight to the star with respect to the upwind direction (θ). The SIMBAD database was utilized to find the V magnitudes, V-K colors, distances (van Leeuwen 2007), and heliocentric radial velocities. The V-K colors are used in the estimation of both the photospheric effective temperatures and stellar radii, based on the prescriptions of Buzzoni et al. (2010) and van Belle (1999), respectively. The radii computed in this manner should have uncertainties of 11.7% (van Belle 1999). Five of the stars have interferometric radii measured by Mozurkewich et al. (2003). The only one initially found to be in poor agreement was μ Gem. The discrepancy was resolved by replacing the initially assumed magnitude with the 2MASS catalog's $K = -1.86$ value (Cutri et al. 2003), changing the V-K color and inferred radius significantly.

In computing the last two quantities of Table 1 regarding the ISM flow direction and magnitude at each star, which

Table 1. HST red giant targets

Star	Alternate Name	Spect. Type	V[a]	V-K[b]	T_{eff}[c] (K)	R[d] ($R_\odot$)	d[e] (pc)	V_{rad}[f] (km/s)	log F_{MgII}[g]	V_w[h] (km/s)	V_{ISM}[i] (km/s)	θ[j] (deg)
New Survey Targets												
HD 66141	HR 3145	K2 III	4.38	2.97	4274	23.9	77.9	71.6	5.08	...	76	142
HD 211416	α Tuc	K3 III	2.82	2.91	4310	37.3	61.2	42.2	5.02	...	52	140
HD 87837	HR 3980	K4 III	4.38	3.34	4086	33.6	90.6	39.8	4.69	...	45	143
HD 50778	θ CMa	K4 III	4.08	3.42	4052	35.4	79.9	96.2	4.96	30 ± 5	95	150
HD 59717	σ Pup	K5 III	3.25	3.66	3959	43.7	59.4	87.3	4.84	43 ± 7	88	147
HD 25025	γ Eri	M1 III	2.94	3.87	3889	58.9	62.3	60.8	4.67	24 ± 7	57	146
HD 44478	μ Gem	M3 III	2.87	4.73	3675	107.7	71.0	54.4	4.50	19 ± 5	55	144
HD 20720	τ^4 Eri	M3.5 III	3.70	4.85	3652	102.9	93.4	41.7	4.49	23 ± 7	34	149
HD 120323	HR 5192	M4.5 III	4.19	5.85	3500	82.4	56.1	40.7	4.20	19 ± 5	43	172
Archival Stars												
HD 124897	α Boo	K2 III	−0.05	2.86	4341	25.2	11.3	−5.2	5.23	43 ± 4	113	92
HD 164058	γ Dra	K5 III	2.23	3.58	3989	53.4	47.3	−27.9	4.79	(74)	18	40
HD 29139	α Tau	K5 III	0.86	3.90	3880	51.0	20.4	54.3	4.77	35 ± 5	44	170
HD 108903	γ Cru	M3.5 III	1.64	4.76	3669	73.9	27.2	21.0	4.49	28 ± 9	37	116

NOTE—[a]V band magnitude. [b]V-K color. [c]Photospheric effective temperature. [d]Stellar radius. [e]Stellar distance. [f]Heliocentric radial velocity. [g]Logarithmic Mg II h & k surface flux (in ergs cm^{-2} s^{-1} units). [h]Stellar wind velocity measured from the Mg II k line. [i]Interstellar wind velocity seen by the star in the stellar rest frame. [j]Angle between the upwind direction of the ISM flow vector in the rest frame of the star and our line of sight to the star.

are relevant for astrospheric studies, we note that our target stars are all close enough to be within the Local Bubble (LB), a region of generally low ISM density extending roughly 100 pc from the Sun in most directions (Sfeir et al. 1999; Lallement et al. 2003). We verify that the stars are within the LB using the LB maps of Lallement et al. (2003). Most of the volume of the LB is believed to be very hot, ionized plasma, which produces much of the soft X-ray background emission (Snowden et al. 1998, 2014). The flow vector of the LB material is uncertain, but a plausible assumption is that it is roughly at rest relative to the Local Standard of Rest (LSR) (e.g., Dehnen & Binney 1998). Combining this assumption with the known proper motion and radial velocity of our target stars, we can estimate the ISM flow vector seen in the rest frame of the star and its orientation relative to our line of sight to the star, characterized by the V_{ISM} and θ parameters in Table 1. All the new survey stars have $\theta \geq 140°$, confirming that the lines of sight to these stars are expected to be very downwind, which was one of the desired selection criteria to maximize the likelihood of detecting astrospheric absorption.

The nine newly observed stars were observed by the Space Telescope Imaging Spectrograph (STIS) instrument on HST (Kimble et al. 1998; Woodgate et al. 1998), with the observations occurring between 2013 October and 2015 January. For each of our targets, the HST visit consisted of a spectrum of the 2574–2851 Å wavelength range taken with STIS's high resolution ($R \equiv \lambda/\Delta\lambda = 110,000$) E230H grating, followed by a longer exposure of the 1150–1700 Å wavelength range taken with the moderate resolution ($R = 46,000$) E140M grating. Our focus here is on the Mg II h & k lines within the E230H spectrum, with rest wavelengths of 2803.5315 Å and 2796.3543 Å, respectively (Morton 2003). The α Tau spectrum considered is the same as that studied by Wood et al. (2007), which is from 1994 April 8, and is a product of the Ech-B grating on the UV spectrometer that preceded STIS on HST, the Goddard High Resolution Spectrograph (GHRS). The other three archival Mg II spectra considered are all STIS/E230H observations, from 1998 August 24, 2011 August 11, and 2011 August 4 for α Boo, γ Dra, and γ Cru, respectively.

Figure 1 displays the Mg II spectra of all the K2-M5 III stars listed in Table 1, in spectral type order. We also include in the figure an archival HST/GHRS Mg II spectrum of the K0 III star β Gem (Dring et al. 1997). Being on the coronal side of the dividing line mentioned in section 1, the β Gem spectrum serves to illustrate what a red giant chromospheric Mg II line profile should look like in the absence of an opaque stellar wind. The stellar rest frame is indicated in Figure 1, but for two stars in our sample that are spectroscopic binaries the figure instead indicates the systemic center-of-mass radial velocity and the range of velocities covered by the red giants in their elliptical orbits.

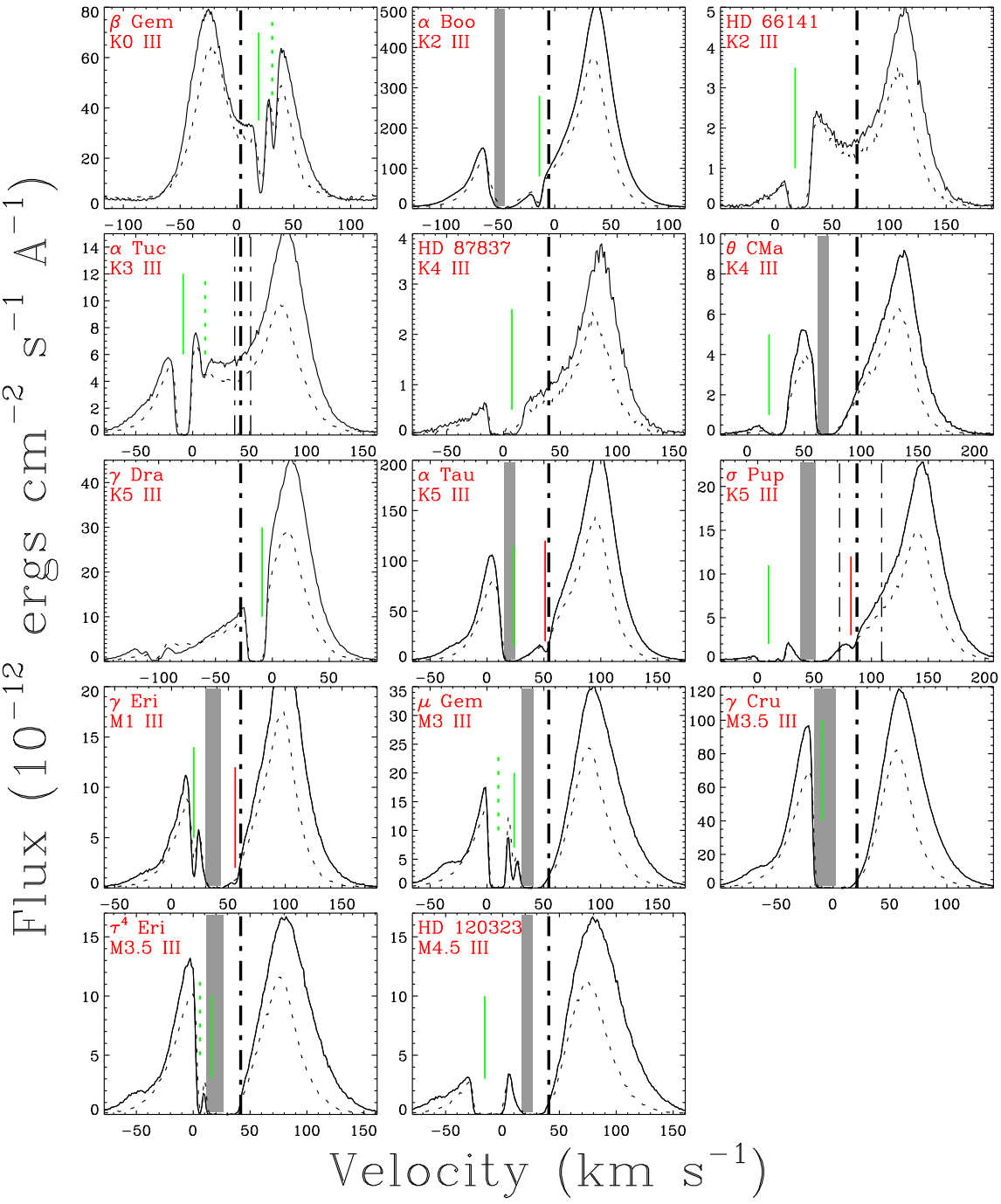

Figure 1. Mg II h (dotted) and k (solid) lines observed by HST are plotted on a heliocentric velocity scale, with the stars shown in order of spectral type. Although not actually in our sample of K2-M5 III stars, β Gem (K0 III) is included here to illustrate what Mg II profiles look like for a coronal giant without a strong wind. Thick vertical dot-dashed lines indicate the stellar rest frame (V_{rad}), although for two stars in spectroscopic binary systems (α Tuc and σ Pup) it is actually the systemic center-of-mass velocity, and the thin dot-dashed lines around it mark the range of orbital motion of the red giant. Green lines indicate ISM absorption features, with solid lines marking the expected location of LIC absorption, and dotted lines identifying other absorption that we believe is from the ISM. Shaded regions indicate the estimated stellar wind terminal velocity and its uncertainty, for stars with deep, opaque wind absorption. Red lines mark astrospheric absorption; only seen for α Tau, σ Pup, and γ Eri.

These two systems are α Tuc (K3 III+?) and σ Pup (K5 III+G5 V), with orbital periods of 4197.7 and 257.8 days, respectively (Pourbaix et al. 2004). The actual radial velocities of the red giants at the times of observation are best estimated from narrow H_2 lines in the FUV E140M spectrum, which suggest radial velocities of 42 and 103 km s^{-1} for α Tuc and σ Pup, respectively. The implications of σ Pup's binarity will be discussed in detail in section 6.

The Mg II profiles are complicated by the presence of intervening absorbers in between the stellar chromosphere and the observer. These absorbers include the stellar wind, the ISM, and the stellar astrosphere. Given that all our stars are relatively nearby, we expect the ISM absorption to be relatively close to the velocity predicted by the local interstellar cloud (LIC) vector measured for the ISM cloud immediately surrounding the Sun (e.g., Redfield & Linsky 2008; Wood et al. 2015). Multiple ISM velocity components are often observed even for very nearby stars, but not typically at velocities separated by more than $\sim$ 20 km s^{-1} from the LIC velocity (Redfield & Linsky 2002).

The LIC velocity is shown explicitly in all the Figure 1 panels. There is always absorption observed at that location. Although the figure identifies the absorption as LIC, there could be a blend of ISM velocity components, particularly in cases like HD 87837 where the absorption feature is particularly broad and not well centered on the LIC velocity. In several cases (α Tuc, μ Gem, and τ^4 Eri) there is a separate, distinct narrow absorption feature adjacent to the LIC absorption that we suspect is interstellar, and it is identified as such in Figure 1. Our selection of stars with high, positive radial velocities shifts the stellar wind absorption redward of the ISM absorption in all cases, generally far enough to adequately separate the two. Among our new survey targets, only for τ^4 Eri have we ended up with a case where the LIC absorption is clearly within the saturated core of the wind absorption, making it impossible to separate the two and complicating analysis of the absorption.

We compute integrated Mg II h and k line fluxes for all the red giant target stars. We correct for ISM absorption by interpolating a continuum over the ISM features identified in Figure 1. Figure 2a shows the k/h flux ratio plotted versus photospheric temperature. The ratio clearly increases towards later spectral types. The ratio would be 2 in an optically thin plasma, but stellar chromospheres are highly optically thick to Mg II emission, so values less than 2 are always observed (Basri & Linsky 1979; Blanco et al. 1982; Cerruti-Sola et al. 1992). The spectral type dependence of k/h seen in Figure 2a, which is not seen for main sequence stars, is indicative of systematic changes in the chromospheric opacity towards the later type giants, which will have lower surface gravities due to larger radii (see Table 1). Past solar and stellar chromospheric models have discussed the diagnostic potential of the k/h ratio (e.g., Linsky & Avrett 1970; Leenaarts et al. 2013).

After summing up the flux of both the h and k lines, we can compare the HST fluxes with those measured previously by the *International Ultraviolet Explorer* (IUE). For the eight stars we have in common with the Pérez Martínez et al. (2011) compilation of evolved star IUE Mg II fluxes we find reasonably good agreement, with no systematic flux discrepancies, and an average difference of only 20.8%. We convert the fluxes at Earth to surface fluxes (F_{MgII}) in ergs cm^{-2} s^{-1} units, which are listed logarithmically in Table 1. The biggest uncertainty in the surface fluxes lies in the stellar radii. The 11.7% angular diameter uncertainty from van Belle (1999) translates into a 23.4% error in F_{MgII}, which leads to 0.09 dex uncertainties for the log F_{MgII} values in Table 1.

In Figure 2b, the Mg II fluxes are plotted versus temperature. There is a strong correlation, and a simple line fits the data quite well, suggesting

$$\log F_{\rm MgII} = 9.109 \log T_{eff} - 28.000. \quad (1)$$

The correlation is apparent whether F_{MgII} is plotted versus spectral type, V-K, or temperature. The 1σ scatter about the fitted line is only 0.054 dex, or about 13%, which is less than the 23.4% F_{MgII} uncertainty estimated above. The remarkably tight correlation between chromospheric activity and temperature (or spectral type) seen for red giants is very different from what is found for main sequence stars. For main sequence stars, the Mg II fluxes span a range of about a factor of 30 at a given spectral type, due to chromospheric and coronal emission being largely determined by rotation rate, which can vary greatly (e.g., Mathioudakis et al. 1995; Ribas et al. 2005; Wood et al. 2005b).

The homogeneity of K2-M5 III Mg II fluxes at a given spectral type is consistent with the idea that on the noncoronal side of the dividing line giant stars are all rotating very slowly, and at a given spectral type the stars are therefore producing chromospheric emission at basically the same basal flux level (Schrijver 1987; Pérez Martínez et al. 2011). We found rotational velocity measurements for eight of our thirteen stars (De Medeiros & Mayor 1999; De Medeiros et al. 2014), and all are slow rotators. Only σ Pup has a rotational velocity above 2 km s^{-1}, with $v \sin i = 2.9 \pm 1.1$ km s^{-1}. In Figure 2b, our Mg II fluxes are compared with the "V-K Model" basal flux line of Pérez Martínez et al. (2011), based on IUE measurements of many more stars over a wider range of spectral types, albeit with many coronally active stars not emitting at a basal level. There is reasonably good agreement, though our measurements suggest a slightly steeper relation, $F_{\rm MgII} \propto T_{eff}^{9.1}$ instead of $F_{\rm MgII} \propto T_{eff}^{6.8}$, at least in this spectral type range.

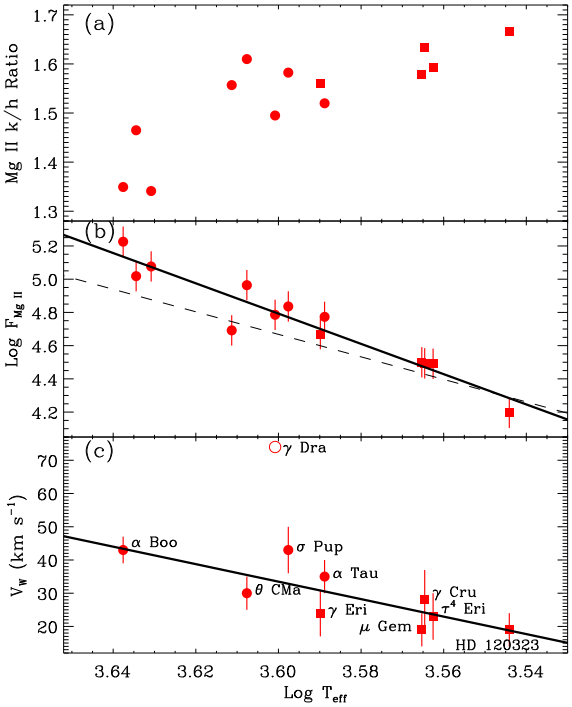

Figure 2. (a) Mg II k/h flux ratio plotted versus photospheric temperature for K (circles) and M (squares) giants. (b) Mg II surface fluxes versus photospheric temperature, with a linear fit. The dashed line is the "V-K Model" basal flux line of Pérez Martínez et al. (2011). (c) Stellar wind velocity versus temperature, with a linear fit that excludes the discrepant γ Dra.

One paradigm for the basal chromosphere phenomenon is that it represents the chromospheric heating level due to the dissipation of acoustic waves generated from photospheric oscillations, and in the absence of significant magnetic activity this is the dominant chromospheric heating mode (Buchholz et al. 1998; Rammacher & Cuntz 2003; Ulmschneider et al. 2005; Cuntz et al. 2007). Acoustic heating models appear to be able to successfully reproduce the observed dependence of basal flux on photospheric temperature, a dependence that is similar on both giants and main sequence stars. However, alternative views exist, which suggest that a base level of magnetic activity is instead responsible (e.g., Judge & Carpenter 1998). Support for this view comes from the existence of a basal level of coronal X-ray emission for main sequence stars, which it is widely accepted requires a magnetic origin (Stepien & Ulmschneider 1989; Schmitt 1997; Schröder et al. 2012). It is less clear that a basal X-ray emission level exists for K2-M5 III stars, as so few have reliable X-ray detections (Ayres et al. 2003). Nevertheless, the detection of magnetic fields on the supergiant Betelgeuse (Aurière et al. 2010) and the Mira χ Cyg (Lèbre et al. 2014), as well as the observation of an X-ray outburst on Mira itself (Karovska et al. 2005), demonstrates that even very cool, evolved, and slowly rotating stars still have some magnetic activity, and many models of red giant chromospheres and wind acceleration rely on the presence of magnetic fields and Alfvén waves (Suzuki 2007; Airapetian et al. 2010).

3. THE STELLAR WIND ABSORPTION PROFILES

Even in the absence of the ISM absorption, wind scattering, and astrospheric absorption, the Mg II line profiles are already complex due to the high opacity of the chromospheric Mg II lines. The β Gem line profile in Figure 1 is double-peaked, with a stronger blue peak. Such "self-reversals" are typical for chromospheric Mg II lines, including ones observed from the Sun, and the blue peak is commonly found to be the stronger one (Donnelly et al. 1994). None of the K2-M5 III Mg II profiles are like that of β Gem. The closest are the spectra of HD 66141 (K2 III) and α Tuc (K3 III), which might be interpreted as being chromospheric lines that happen to have stronger red peaks, but it is far more likely that this shift in flux from blue peak to red peak is an indication of a chromospheric wind scattering flux from the blue side of the line to the red.

The wind will naturally be most opaque just bluewards of the stellar rest frame, extending to the wind's terminal velocity, and even beyond it to an extent determined by the turbulent velocities in the wind at its terminal speed. The wind will be a photon-scattering environment in which Mg II photons absorbed and reemitted by Mg^+ ions in the wind will preferentially escape by frequency scattering away from the velocities at which the wind is most opaque (e.g., Harper et al. 1995). For most of the stars in Figure 1, the result is a broad, deep, saturated wind absorption feature blueward of the stellar rest frame.

However, for three of the stars close to the dividing line at K2-K4 III (HD 66141, α Tuc, and HD 87837) the wind is apparently weaker and less opaque, and the effect on the line profile is more subtle, yielding merely a line asymmetry with more flux emerging redward of the stellar rest frame. The exception is the well-studied K2 III star α Boo, which shows deep wind absorption despite being very close to the coronal dividing line, implying a high mass loss rate of $\dot{M} = 2 \times 10^{-10}$ M$_\odot$ yr^{-1} (O'Gorman et al. 2013).

For the stars that have deep wind absorption, we can estimate the terminal wind speed (V_w) empirically, based on the following prescription. First, we determine the maximum flux level within the Mg II k line blueward of the stellar rest frame (e.g., $\sim 5 \times 10^{-12}$ ergs cm^{-2} s^{-1} Å^{-1} for θ CMa). Second, we divide this value by an admittedly arbitrary factor of 20, and we then determine at what velocity that flux level is reached on the blue side of the wind absorption (V_b). In the stellar rest frame, this represents an upper bound for V_w. Next, we determine at what velocity that flux level is reached on the red side of the wind absorption (V_r). The average of V_b and V_r represents an estimate of the center of the wind absorption, which in the stellar rest frame provides an estimate of the lower bound of V_w. The shaded regions in Figure 1 indicate the range of V_w implied by these lower and upper bounds for all the stars. If microturbulent velocities in the stellar wind at the terminal velocity are low (e.g., a few km s^{-1}) then the upper bound (i.e., the left edge of the shaded region) should be close to V_w; but if turbulent velocities are high then the lower bound (i.e., the right edge of the shaded region) would be a better estimate (Harper et al. 1995). In any case, with the bounds on V_w now defined, we can now quote an estimate of V_w with error bars, which are listed in Table 1. Mathematically, if V$_b$ and V$_r$ are in a heliocentric rest frame, as in Figure 1, then $V_w = V_{rad} - [V_b + (V_r - V_b)/4]$, with uncertainty $\Delta V_w = (V_r - V_b)/4$.

We cannot use this prescription for the first three giants listed in Table 1, which do not have the deep, saturated wind absorption features (see Figure 1). The K5 III giant γ Dra is a special case. It does not possess a broad, deep stellar wind absorption feature, but there is a rather narrow dip at a heliocentric velocity of -102 km s^{-1} in Figure 1, which is likely indicative of the wind terminal velocity. This implies a very high wind speed of $V_w = 74$ km s^{-1}. An older HST/GHRS spectrum of γ Dra studied by Robinson et al. (1998) shows a similar profile, but with the absorption feature less blueshifted, suggesting $V_w = 67$ km s^{-1}. However, Robinson et al. (1998) find it difficult to interpret the Mg II profile with a single wind component, and propose the existence of a slower wind component (with $V_w = 30$ km s^{-1}) in addition to the fast one producing the narrow absorption dip. The speed of this slower wind component is more consistent with that observed for the other K giants.

The Mg II profiles of γ Dra are in most respects similar to those of HD 87837 (K4 III), but HD 87837 does not have the absorption dip far from the stellar rest frame that would suggest that there is necessarily opaque stellar wind material at those high speeds. It is tempting to associate γ Dra's unusually fast wind with the star also being one of the most well-known hybrid-chromosphere giants, with weak but detectable coronal X-ray emission (Ayres et al. 2006), and detectable transition region UV emission from lines such as C IV λ1548 (Ayres et al. 1997). Harper et al. (1995) found a very high wind speed of $V_w = 104$ km s^{-1} for α TrA (K4 II), which is another canonical hybrid chromosphere star. Before the HST era, Reimers (1982) previously noted a possible correlation between the hybrid chromosphere stars and high speed Mg II wind absorption features in IUE spectra. Thus, both the HST and IUE databases of red giant spectra seem to be consistent with the notion that red giants with unusually strong transition region and coronal emissions also have high speed wind components.

The wind velocities of the M giants are clearly lower than those of the K giants in our sample, with $V_w \sim 40$ km s^{-1} for K2 III stars near the coronal dividing line, and $V_w \sim 20$ km s^{-1} at M5 III. The correlation is shown explicitly in Figure 2c, which plots V_w versus photospheric temperature. Excluding the clearly discrepant γ Dra, the linear fit is

$$V_w = 263.16 \log T_{eff} - 913.90. \quad (2)$$

This is the clearest demonstration of such a correlation for red giants, though past Mg II observations from IUE have also suggested a trend of this nature (Drake 1986; Drake & Linsky 1986; Judge & Stencel 1991).

There is some ambiguity with regards to whether the optical spectra of Ca II H & K wind absorption support a wind velocity correlation with spectral type. The wind velocities quoted by Reimers (1977) would seem to suggest lower velocities for M giants, but inferences of terminal velocities from the Ca II data are open to interpretation. At least within the M giants alone, which are the only class III stars with reliably deep, saturated wind absorption, the centroid velocity of the Ca II absorption decreases towards later spectral types but the blueward extent of the absorption does not, leading to the early interpretation that these variations are indicative of changes in line formation depth and turbulent velocity with spectral type rather than any change in wind velocity (Deutsch 1960; Reimers 1975; Boesgaard & Hagen 1979). The very presence of Ca II wind absorption implies that the stellar wind must be relatively cold close to the star.

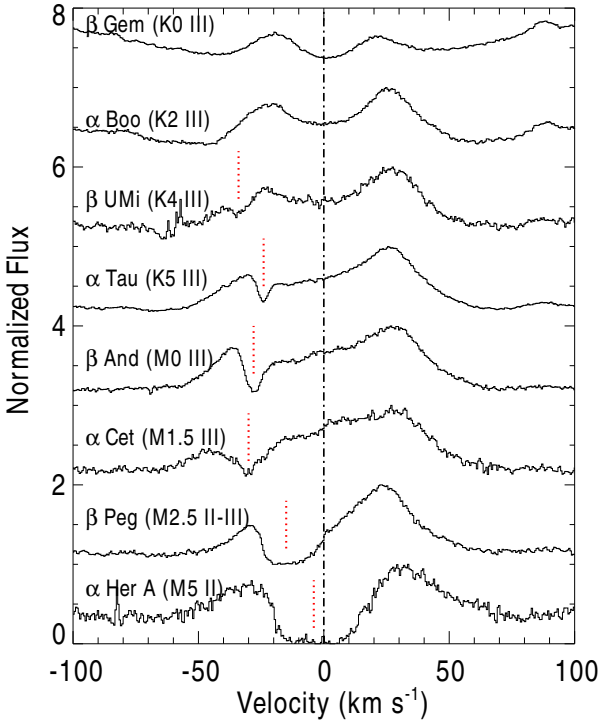

Figure 3. Ca II K line profiles of 8 evolved stars, observed by the Harlan J. Smith Telecope at McDonald Observatory. The spectra are shown on a velocity scale centered on the rest frame of the star (dot-dashed line). For all stars except β Gem, wind scattering leads to a red peak stronger than the blue peak, and in most cases to clear absorption features marked with dotted lines.

We can further explore the comparison of Ca II and Mg II wind diagnostics using more recent Ca II observations, specifically spectra taken at a very high resolution of $R = 200,000$ with the Coude cross-dispersed spectrometer (cs21) on the 2.7-meter Harlan J. Smith Telecope at McDonald Observatory. In 2006 January, eight K0-M5 evolved stars were observed: β Gem (K0 III), α Boo (K2 III), β UMi (K4 III), α Tau (K5 III), β And (M0 III), α Cet (M1.5 III), β Peg (M2.5 II-III), and α Her A (M5 II). The spectral type range covered resembles our HST red giant sample, although the last two stars drift out of luminosity class III. Figure 3 shows the resulting spectra of the Ca II K line.

Analogous to Figure 1, β Gem is used in Figure 3 to indicate what the Ca II line profile looks like for a coronal star without a strong chromospheric wind, and as for Mg II, the line profile is double-peaked, with a stronger blue peak. All of the other Ca II K lines in Figure 3 have stronger red peaks, suggesting the presence of a wind. However, the latest type stars, β Peg and α Her A, are the only ones that exhibit deep, saturated Ca II wind absorption profiles. The wind signatures are more subtle for the earlier type stars. The α Boo and β UMi Ca II profiles are very similar to the Mg II profiles of HD 66141 and α Tuc (see Figure 1). It is interesting that α Boo, which has strong and deep Mg II wind absorption in Figure 1, does not exhibit analogously strong Ca II absorption in Figure 3. Several of the stars (α Tau, β And, α Cet, and perhaps β UMi) show relatively narrow, weak Ca II absorption between -34 and -24 km s^{-1} that should be indicative of the stellar wind's terminal speed. These features resemble the narrow Mg II absorption seen in Figure 1 for γ Dra, albeit not at nearly as high a velocity. The -34 to -24 km s^{-1} range of velocities is comparable to the wind speeds inferred from Mg II.

However, it is worth noting that for α Tau, we inferred $V_w = 35 \pm 5$ km s^{-1} from Mg II, while the α Tau Ca II absorption in Figure 3 would suggest a lower value of $V_w \approx 24$ km s^{-1}. This is likely due to actual variability in the wind of α Tau. The variability of the Ca II wind absorption seen from α Tau has long been established (Reimers 1977; Kelch et al. 1978). More recently, Harper et al. (2011) found the wind velocity inferred from Ca II wind absorption to increase from 20.9 to 28.0 km s^{-1} between 2005 September and 2007 March.

4. NEW ASTROSPHERIC ABSORPTION DETECTIONS

Based on the α Tau example, astrospheric Mg II absorption should be weak, narrow, and slightly blueshifted from the stellar rest frame. Only two of the other stars in our sample, σ Pup and γ Eri, show absorption of this nature (see Figure 1). We not only look for astrospheric absorption in the Mg II lines, but also in other lines within our HST spectra in which it might be observed, particularly the O I line at 1302.2 Å, C II at 1334.5 Å, and Fe II at 2600.2 Å,

Table 2. Astrospheric Absorption Line Measurements

Star	Species	V[a] (km/s)	b[b] (km/s)	log N[c]	η[d]	T[e] (10^4 K)
σ Pup	Mg II	83.7 ± 0.1	3.88 ± 0.16	12.064 ± 0.012	11.9 ± 2.1	2.19 ± 0.18
	Fe II	85.0 ± 0.8	2.9 ± 1.5	12.38 ± 0.17	...	...
	C II	82.9 ± 1.8	4.9 ± 3.1	13.47 ± 0.20	...	...
γ Eri	Mg II	56.7 ± 0.1	2.51 ± 0.13	12.213 ± 0.013	5.9 ± 1.7	0.92 ± 0.09
	Fe II	56.1 ± 1.5	1.1 ± 1.7	12.15 ± 0.38	...	...
α Tau	Mg II	52.3 ± 0.1	3.55 ± 0.04	12.230 ± 0.003	17.5 ± 3.1	1.83 ± 0.04

NOTE—[a]Heliocentric velocity. [b]Doppler broadening paramter. [c]Logarithmic column density (in cm^{-2} units). [d]Termination shock compression ratio. [e]Post termination shock temperature.

which all have line profiles similar to Mg II, with the deep wind absorption trough. For γ Eri we find a marginal detection of Fe II absorption, while for σ Pup we find more convincing detections for both Fe II and C II. Given that for α Tau the absorption signature was only seen in Mg II, these are the first detections of the astrospheric absorption signature in any line but Mg II. Figure 4 displays all astrospheric absorption lines detected to date, for all three red giants with detected astrospheres.

We have fitted these absorption features with single absorption lines, analyzing them in the same fashion as ISM absorption lines (e.g., Redfield & Linsky 2002, 2004). Required oscillator absorption strengths are taken from Morton (2003). Each absorption component is defined by three parameters: central velocity (V), Doppler broadening parameter (b), and column density (N). To constrain the fit as much as possible, the two Mg II lines are fitted simultaneously, with self-consistent fit parameters. The resulting fits to the data are shown in Figure 4, taking into account instrumental broadening using line spread functions from Hernandez et al. (2012). The fit parameters are listed in Table 2. The column densities, with units of cm^{-2}, are listed in logarithmic form. The Fe II and C II data are noisy, and the C II line is not well resolved in the E140M spectrum. As a consequence, uncertainties in the Fe II and C II fit parameters are large.

The velocities of the astrospheric absorption listed in Table 2 indicate the post-TS velocity, after being subtracted from V_{rad} to place them in the proper stellar rest frame. The V_w velocities in Table 1 are the pre-TS velocities. The ratio of the two is a measure of the compression ratio (η) of the TS. Mathematically, $\eta = V_w/[V_{rad} - V(\mathrm{MgII})]$. The η values of the three detected astrospheres are listed in Table 2.

Assuming the absorption line widths are dominated by thermal broadening, the Doppler parameters (in km s^{-1}) will be related to temperature by $b^2 = 0.0165T/A$, where A is the atomic weight of the species in question. The last column of Table 2 lists temperatures computed from this equation using the Mg II Doppler parameters (with $A = 24$).

If the TS is radiative, some of the astrospheric absorption may be coming from the intermediate radiative relaxation zone of the shock, rather than being entirely from post-TS material that has reached its final flow velocity and temperature. The effects of velocity gradients in this region would be to broaden the absorption line and shift the line centroid blueward of the true terminal post-TS velocity. This would mean that η in Table 2 could actually be an underestimate and T an overestimate. However, velocity gradients in the relaxation region should also induce asymmetries in the absorption profiles, for which we do not see any evidence, which is an argument in favor of the absorption being dominated by post-relaxation zone material.

At the TS, the kinetic energy of the stellar wind is partly converted to thermal energy in the post-TS material. Thus, there should be a correlation between V_w and the temperatures listed in Table 2. We can be more specific using the conservation of momentum equation of the Rankine-Hugoniot shock jump relations, which says

$$P_1 + \rho_1 v_1^2 = P_2 + \rho_2 v_2^2, \tag{3}$$

where P_1, ρ_1, and v_1 are the pressure, density, and velocity upstream of the shock; and P_2, ρ_2, and v_2 are the corresponding quantities downstream. An MHD version of equation (3) would include $B^2/8\pi$ terms, but such terms should not be significant here. In the strong shock limit appropriate here, P_1 is negligible and $\eta = \rho_2/\rho_1 = v_1/v_2 = 4$ for a simple hydrodynamic shock (e.g., Shu 1992). Thus, equation (3) reduces to

$$P_2 = \frac{3}{4}\rho_1 v_1^2. \tag{4}$$

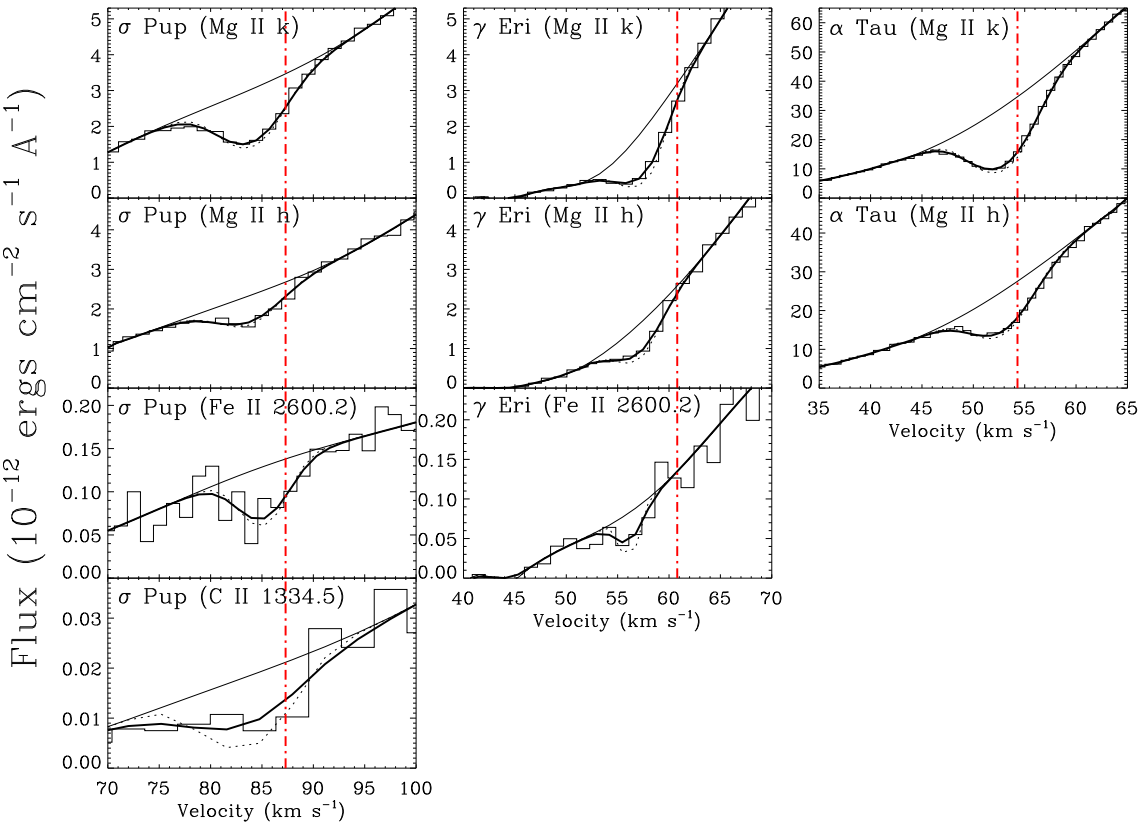
σ Pup (Mg II k)
γ Eri (Mg II k)
α Tau (Mg II k)
σ Pup (Mg II h)
γ Eri (Mg II h)
α Tau (Mg II h)
σ Pup (Fe II 2600.2)
γ Eri (Fe II 2600.2)
σ Pup (C II 1334.5)
Flux (10^-12 ergs cm^-2 s^-1 A^-1)
Velocity (km s^-1)

Figure 4. Fits to astrospheric absorption lines observed towards σ Pup (left), γ Eri (middle), and α Tau (right), plotted on a heliocentric velocity scale. Dotted and solid lines show the fits before and after convolution with the instrumental line profiles, respectively. Vertical dot-dashed lines indicate the stellar rest frame.

The post-TS pressure and temperature are related by $P_2 = n_2 k_B T_2$, where k_B is the Boltzmann constant and n_2 the number density. For a pure hydrogen fluid, $\rho_1 = m_p n_1$, where m_p is the proton mass. Plugging these relations into equation (4) and noting that $n_2/n_1 = \eta = 4$ leads to

$$T_2 = 22.7 v_1^2, \tag{5}$$

if v_1 is in km s^{-1} units.

In Figure 5, we plot this expected relation between stellar wind speed and post-TS temperature, which is compared with the actual measurements for the three detected astrospheres. We do see an increase in temperature with V_w, but the measured temperatures are lower than predicted. The explanation for the discrepancy lies in the assumption of a simple hydrodynamic shock in deriving equation (5), which requires $\eta = 4$ in the strong shock limit. However, from Table 2 we already know $\eta > 4$ for all three detected astrospheres. This is evidence for a dissipative shock, as suggested before for α Tau, where the astrospheric absorption could only be reproduced when the TS was modeled as a radiative shock (Wood et al. 2007). The dashed line is representative of the initial post-TS temperature, but radiative cooling decreases this temperature, resulting in additional compression. It is worth noting that the star with the lowest η, γ Eri, is not surprisingly closest to the expected temperature in Figure 5. For γ Eri, less radiative cooling and associated compression is necessary to reach the observed temperature. This is explored further with a full hydrodynamic model of the γ Eri astrosphere in the next section.

A final question to address in this section concerns the issue of why only three of the red giant targets in Table 1 show the astrospheric absorption signature. The θ values of the three archival nondetections (α Boo, γ Dra, and γ Cru) demonstrate that we are not looking through the astrotail, and therefore we may not have sufficient Mg II column densities along the lines of sight to these stars to detect astrospheric absorption. This, however, is not true for the 7 new targets that did not yield detections.

One problem for the three M3-M5 giants in that list (μ Gem, τ^4 Eri, and HD 120323) is that there is very little flux near the stellar rest frame to provide a suitable background for the astrospheric signature, making it harder to detect. This is presumably due to a combination of low wind speed and high mass loss rate. As discussed above with regards to γ Eri, the low wind speed also reduces the heating at the TS, thereby reducing radiative cooling and

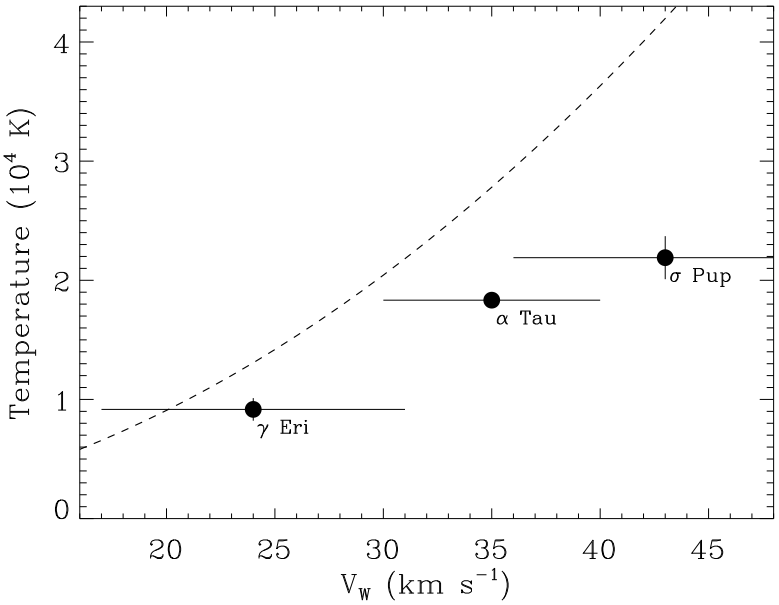

Figure 5. The post-TS temperature estimated from the astrospheric Mg II lines in Table 2 is plotted versus the stellar wind velocity estimates from Table 1. The dashed line is the relation expected for a simple hydrodynamic shock at the strong shock limit, assuming a pure hydrogen fluid.

post-TS compression, which also reduces astrospheric detectability.

Three of the K2-K4 giants among the nondetections (HD 66141, α Tuc, and HD 87837) have winds weak enough that there is no deep, broad wind absorption feature in the Mg II lines. Perhaps for these stars the winds are not strong enough to carve out astrospheres that are sufficiently large to yield enough post-TS Mg II column density for an astrospheric absorption detection. This does not explain the θ CMa nondetection, though. The θ CMa nondetection is the hardest to explain, as there is strong wind absorption in the Mg II profiles, there is plenty of flux near the stellar rest frame to provide background for the astrospheric signature, and the V_w and θ values for the star are both large enough to expect a detection. In any case, given that only 2 of the 9 stars in our new survey yielded astrospheric detections, despite an effort to choose targets likely to provide detections, it is clear that detectable astrospheric absorption signatures are the exception and not the rule for red giants, even in high quality spectra.

5. THE γ ERI ASTROSPHERE

We compute a hydrodynamic model of the γ Eri astrosphere in much the same manner as we modeled the α Tau astrosphere (Wood et al. 2007). This is a two-fluid model of a type used to model the heliosphere, in which the plasma and neutrals are treated as two separate, distinct fluids that are allowed to interact through charge exchange processes (Pauls et al. 1995). A first step in the modeling process is to define the boundary conditions for the model, specifically the stellar wind boundary conditions at 1 AU from the star, and the parameters for the surrounding ISM.

For the stellar wind, we model the Mg II wind absorption feature using techniques used in the past (Harper et al. 1995; Wood et al. 2007), leading to a mass loss rate estimate of $\dot{M} \simeq 3 \times 10^{-11}$ M$_\odot$ yr^{-1} and a terminal velocity of $V_w = 20$ km s^{-1}. These values can be used to infer densities at 1 AU from the star, representing the inner boundary condition of the hydrodynamic model. The model only considers hydrogen, expected to be the dominant constituent by number and mass. The ionization state of hydrogen is very uncertain. It is expected to be mostly neutral at the $T \sim 10^4$ K temperature of the wind, but some degree of ionization may be present. We assume a 10% ionization. We assume a temperature of 7500 K for the wind at 1 AU, though this is actually an unimportant parameter given that the flow is very supersonic.

Turning to the interstellar boundary conditions, the ISM flow velocity and direction represented by the V_{ISM} and θ values from Table 1 are necessary constraints. As for density and temperature appropriate for hot LB plasma, we assume a temperature and proton density of $T_\infty = 5 \times 10^5$ K and $n_\infty(\mathrm{H}^+) = 0.01$ cm^{-3}, respectively, as assumed for Model 8 of the α Tau astrosphere from Wood et al. (2007). There are small, partly neutral clouds within the LB, including the LIC surrounding the Sun, but we assume γ Eri will be surrounded by the more typical hot LB plasma.

Figure 6 shows the resulting hydrodynamic model of γ Eri. The figure shows maps of temperature and density. The stellar wind expands radially from the star until it hits the roughly circular TS, at a distance of about 350 AU in the

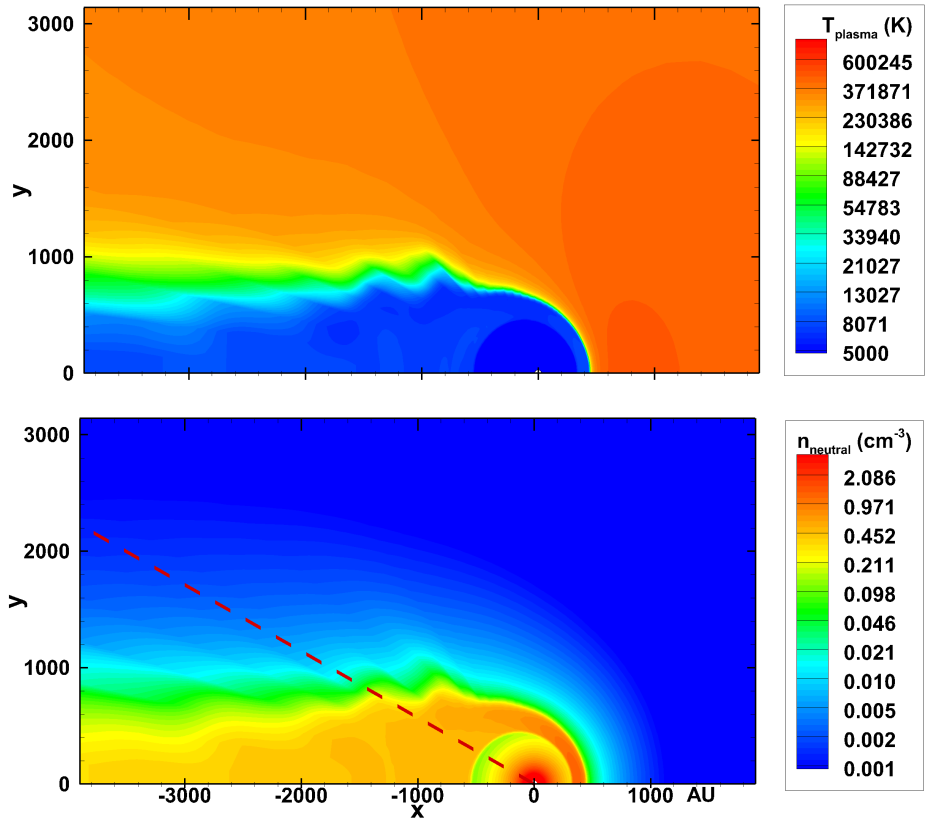

Figure 6. Hydrodynamic model of the γ Eri astrosphere, with top panel showing temperature and the bottom panel showing number density. The dashed line in the bottom panel indicates our line of sight to the star.

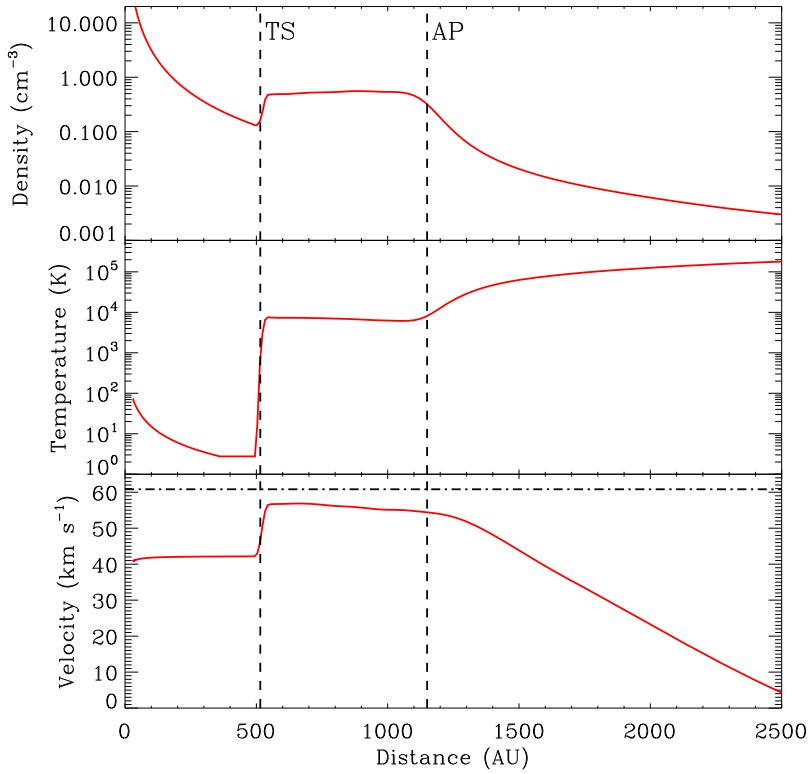

Figure 7. Neutral hydrogen density, temperature, and velocity along the line of sight to the star shown in Figure 6. The dot-dashed line in the bottom panel is the rest frame of the star. The positions of the termination shock (TS) and astropause (AP) are noted.

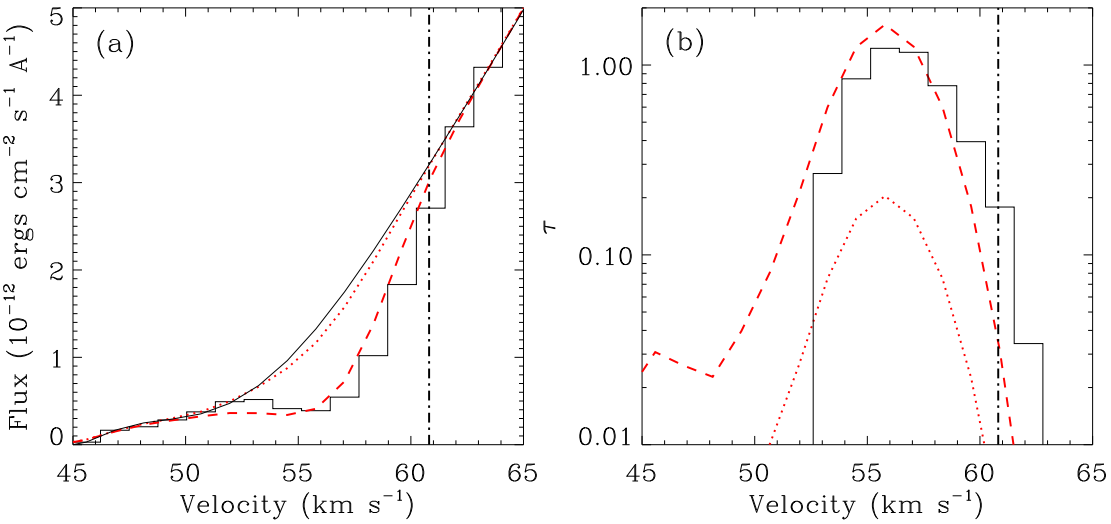

Figure 8. (a) Comparison of observed astrospheric Mg II absorption towards γ Eri (histogram) with the absorption predicted by the model in Figure 6 (dotted line). The dashed line is the predicted absorption after opacities are arbitrarily increased by a factor of 8 to better fit the data. (b) Comparison of observed astrospheric Mg II line opacity with that predicted by the Figure 6 model (dotted line), with the dashed line being the predicted opacity increased by a factor of 8 to better fit the data.

upwind direction and about 550 AU in the downwind direction. The TS is seen most clearly in the density plot in Figure 6. The heated, compressed, and decelerated post-TS wind material is partly deflected downwind towards the astrotail, separated from the plasma flow of the ISM by a parabola-shaped "astropause" (analogous to the heliopause), although the large mean free path of the neutrals allows them to cross this boundary and create the halo of neutrals around it, in green in the density plot of Figure 6. Unlike most heliospheric models, the ISM flow does not pass through a bow shock, as the ISM flow is not supersonic due to the high temperature of the assumed LB plasma.

Figure 7 shows the traces of H I density, temperature, and velocity along our $\theta = 146°$ line of sight to γ Eri. The locations of the TS and astropause in this direction are noted. It is the post-TS material in between the TS and astropause that will be responsible for the astrospheric Mg II absorption feature, as that is where the density is highest. Computing Mg II absorption from the hydrogen parameters in Figure 7 requires that we assume that Mg II is the dominant ionization state of Mg, and we assume a solar Mg abundance (Grevesse & Sauval 1998).

The Mg II absorption predicted by the model is compared with the data in Figure 8a. The model significantly underpredicts the amount of absorption, to the extent that it is difficult to see the difference between the predicted absorption and the assumed background flux above the absorption. Thus, Figure 8b shows a different version of this plot, showing the opacity across the line profile. The model is quite successful in predicting the location and width of the absorption, and if the line opacity is arbitrarily increased by a factor of 8, the predicted absorption actually fits the data reasonably well. The model in Figure 6 is actually more successful in reproducing the observed astrospheric absorption than the hydrodynamic α Tau models, most of which underpredicted the amount of absorption even more severely, and all of which placed the absorption much too far from the stellar rest frame. Treating the α Tau TS as a radiative shock was necessary to increase the amount of absorption and to shift it closer to the stellar rest frame, although even with the radiative shock treatment there was still difficulty predicting a sufficient amount of absorption (Wood et al. 2007).

For γ Eri, the predicted absorption is slightly blueshifted from its observed location, but not by much. This is consistent with the $\eta = 5.9 \pm 1.7$ value reported in Table 2, which indicates a compression ratio slightly higher that the $\eta = 4$ value of a strong, hydrodynamic shock, but not by very much, unlike α Tau. The need to include radiative cooling is therefore much reduced for γ Eri. Including radiative cooling in the γ Eri model, which we will not try here, would presumably improve agreement with the data somewhat, but it is unlikely to be the main reason the model is greatly underestimating the amount of absorption, considering that η is not too much higher than 4 for γ Eri.

Two other possible reasons for the absorption underestimate that are worth considering are: 1. Our assumed Mg abundance in the stellar wind is too low, and 2. The ISM pressure that we are assuming may be too low. As for the first explanation, we are not aware of any precise measurement of a photospheric Mg abundance for γ Eri, but even if such a measurement did exist, the Mg abundance in the stellar wind could be different. Even in the solar wind, the abundances of elements with low first ionization potential can be higher than photospheric abundances by a factor of 4 (von Steiger et al. 1995). Thus, it is plausible that simply assuming a solar photospheric Mg abundance as we have

could be a significant underestimate.

As for the second suggestion, the effects of a high ISM pressure on astrospheric absorption were explored at length in the analysis of the α Tau astrosphere (Wood et al. 2007). Increasing the ISM density pushes the TS closer to the star, where wind densities are higher, leading to the post-TS densities being higher, thereby producing more absorption. In contrast, the amount of astrospheric absorption was unaffected by increases in stellar wind density, because the wind density increase was offset by the effect of pushing the TS farther from the star, where densities are lower. The astrospheric absorption features are therefore potentially useful as ISM pressure diagnostics. The ISM pressure that we are assuming in the γ Eri model ($P/k_B = 5000$ cm^{-3} K) is consistent with measurements of pressures of neutral clouds within the LB (Jenkins 2002), but it may be a little low based on recent assessments of hot plasma within the LB, which suggest $P/k_B = 10,700$ cm^{-3} K (Snowden et al. 2014). Thus, it is possible that an underestimate of the ISM pressure could be part of the explanation for the underestimate of astrospheric absorption.

6. THE σ PUP STELLAR WIND AND ASTROSPHERE

Interpretations of σ Pup's Mg II lines and attempts to model its wind and astrosphere are complicated by its binarity. As noted in section 2, the K5 III giant has a G5 V companion, with an orbital period of 257.8 days. The half-amplitude of the orbital motion is $K1 = 18.6$ km s^{-1} (Pourbaix et al. 2004). This is comparable to the wind speed, so the orbital motion will impart a significant increase in this speed in the direction of orbital motion, and a corresponding decrease in speed in the opposite direction. During the course of one 257.8 day orbit the $V_w = 43$ km s^{-1} stellar wind would travel about 6.5 AU, or about 32 stellar radii. The region around the binary on these distance scales will involve a complex merger of high speed and slow speed streams, with uncertain consequences for the effective final terminal wind speed, although it is expected that the high and slow speed streams will have merged into a more homogeneous outflow before the TS is reached at a distance of ~ 1000 AU. Thus, the systemic center-of-mass velocity quoted as V_{rad} in Table 1 ($V_{rad} = 87.3$ km s^{-1}) is definitely a better reference velocity to use when computing the post-TS velocity and η than the actual stellar radial velocity at the time of the observation, which inspection of narrow H_2 lines in the E140M spectrum suggests is $V_{rad} = 103$ km s^{-1}. The observed astrospheric absorption is certainly close to the former and not the latter.

More questionable is our use of $V_{rad} = 87.3$ km s^{-1} as the reference velocity for computing V_w. Which V_{rad} value is appropriate for estimating V_w depends on whether the wind absorption feature is entirely from the part of the wind close to the star and moving with the star, or whether there is absorption from material farther from the star emitted when the star had a different radial velocity. By assuming $V_{rad} = 87.3$ km s^{-1} we are implicitly assuming the latter, but the former is quite possible. If $V_{rad} = 103$ km s^{-1} is more appropriate, our V_w estimate would increase to $V_w = 59 \pm 7$, which would make σ Pup look discrepant in Figure 2c, albeit still not as discrepant as γ Dra. If σ Pup's Mg II lines could be monitored over the course of an orbit, we could see if the stellar wind absorption precisely follows the star or not, thereby resolving this particular issue. Such monitoring has been done in the optical for the Ca II lines of the spectroscopic binary μ UMa (M0 III+?), with a 230 day period, where it is found that the wind absorption does not seem to follow the radial velocity shifts of the red giant primary (Reimers 1977). This supports our use of the systemic $V_{rad} = 87.3$ km s^{-1} value as the reference velocity in computing V_w, instead of $V_{rad} = 103$ km s^{-1}.

A final complicating factor that should be mentioned concerns the presence of the G5 V companion star, which will be embedded within the wind emitted by the red giant. Gravitational effects on the relatively slow red giant wind could possibly be significant, as could interactions between the winds of the two stars. If the companion star's wind is like that of the Sun, it may be too weak compared with the massive red giant wind to have any effect on the red giant wind, but this is far from certain. In any case, with all these complications in mind, we choose not to compute a σ Pup astrospheric model at this time.

7. SUMMARY

We have analyzed the chromospheric Mg II h & k lines of K2-M5 III stars observed by HST, consisting of 9 observations obtained as part of a new HST red giant survey, and 4 archival targets. Our findings are summarized as follows:

1. The Mg II line profiles of all 13 stars in our sample show evidence for stellar wind absorption, but for three of the K2-K4 III stars the effect is only an induced asymmetry in the line profile rather than a deep wind absorption feature.

2. Measured Mg II surface fluxes are very tightly correlated with spectral type and photospheric temperature, consistent with the idea that K2-M5 III stars redward of the coronal dividing line are all emitting at a basal flux

level. The Mg II k/h flux ratio increases towards later spectral types.

3. Wind speeds estimated empirically from the Mg II spectra correlate with spectral type and photospheric temperature, with V_w decreasing from $V_w \approx 40$ km s^{-1} at K2 III to $V_w \approx 20$ km s^{-1} at M5 III.

4. There are 2 new detections of astrospheric absorption among the recently observed stars (γ Eri and σ Pup), for a total of 3 in our sample, including the previous detection towards α Tau. However, the limited number of new detections indicates that detectable astrospheric absorption in UV lines is not a common phenomenon. For both γ Eri and σ Pup we detect astrospheric Fe II λ2600.2 absorption in addition to the Mg II signature, and for σ Pup, astrospheric absorption is also observed in C II λ1334.5. These are the first detections of red giant astrospheres in lines other than Mg II.

5. Analysis of the astrospheric absorption leads to measurements of TS compression ratio and post-TS temperature for the three detected astrospheres. The temperatures are correlated with V_w. However, the $T = (0.9{-}2.2){\times}10^4$ K post-TS temperatures are too low and the $\eta = 6 - 18$ compression ratios too high according to the Rankine-Hugoniot shock jump conditions, providing further evidence that red giant termination shocks are radiative shocks rather than simple hydrodynamic shocks.

6. We compute a hydrodynamic model of the γ Eri astrosphere, which is the one with the TS compression ratio ($\eta = 5.9 \pm 1.7$) closest to the strong hydrodynamic shock value of $\eta = 4$. Not surprisingly, this model has less difficulty reproducing the observed absorption than was the case for a past study of the α Tau astrosphere (Wood et al. 2007), for which $\eta = 17.5 \pm 3.1$. The γ Eri model places the absorption at about the right velocity and with about the correct width, but it underpredicts the Mg II opacity by a factor of 8. This might be due to either an underestimate of the Mg abundance in the stellar wind, or an underestimate of the ISM pressure surrounding the star.

We would like to thank Drs. Seth Redfield and Alexander Brown for contributing to the acquisition and analysis of the Ca II spectra. Support for HST program GO-13462 was provided by NASA through an award from the Space Telescope Science Institute, which is operated by the Association of Universities for Research in Astronomy, Inc., under NASA contract NAS 5-26555. This research has made use of the SIMBAD database, operated at CDS, Strasbourg, France.

REFERENCES

Airapetian, V., Carpenter, K. G., & Ofman, L. 2010, ApJ, 723, 1210
Aurière, M., Donati, J. -F., Konstantinova-Antova, R., et al. 2010, A&A, 516, L2
Ayres, T. R., Brown, A., & Harper, G. M. 2003, ApJ, 598, 610
Ayres, T. R., Brown, A., & Harper, G. M. 2006, ApJ, 651, 1126
Ayres, T. R., Brown, A., Harper, G. M., et al. 1997, ApJ, 491, 876
Basri, G. S., & Linsky, J. L. 1979, ApJ, 234, 1023
Blanco, C., Bruca, L., Catalano, S., & Marilli, E. 1982, A&A, 115, 280
Boesgaard, A. M., & Hagen, W. 1979, ApJ, 231, 128
Buchholz, B., Ulmschneider, P., & Cuntz, M. 1998, ApJ, 494, 700
Buzzoni, A., Patelli, L., Bellazzini, M., Fusi Pecci, F., & Oliva, E. 2010, MNRAS, 403, 1592
Cerruti-Sola, M., Cheng, C.-C., & Pallavicini, R. 1992, A&A, 256, 185
Cuntz, M., Rammacher, W., & Musielak, Z. E. 2007, ApJ, 657, L57
Cutri, R. M., Skrutskie, M. F., van Dyk, S., et al. 2003, yCat, 2246, 0
De Medeiros, J. R., Alves, S., Udry, S., et al. 2014, A&A, 561, A126
De Medeiros, J. R., & Mayor, M. 1999, A&AS, 139, 433
Dehnen, W., & Binney, J. J. 1998, MNRAS, 298, 387
Deutsch, A. J. 1960, in Stellar Atmospheres, ed. J. L. Greenstein (Chicago: University of Chicago Press), 543.
Donnelly, R. F., White, O. R., & Livingston, W. C. 1994, Sol. Phys., 152, 69
Drake, S. A. 1986, in New Insights in Astrophysics: Eight Years of UV Astronomy with IUE (ESA SP-263), 193
Drake, S. A., & Linsky, J. L. 1986, AJ, 91, 602
Dring, A. R., Linsky, J., Murthy, J., et al. 1997, ApJ, 488, 760
Grevesse, N., & Sauval, A. J. 1998, Space Sci. Rev., 85, 161
Haisch, B., Schmitt, J. H. M. M., & Rosso, C. 1991, ApJ, 383, L15
Harper, G. M., Brown, A., & Redfield, S. 2011, in 16th Cambridge Workshop on Cool Stars, Stellar Systems, and the Sun, ed. C. M. Johns-Krull, M. K. Browning, & A. A. West (San Francisco: ASP), 1145
Harper, G. M., Wood, B. E., Linsky, J. L., et al. 1995, ApJ, 452, 407
Hernandez, S., Aloisi, A., Bohlin, R., et al. 2012, STIS Instrument Handbook, Version 12.0 (Baltimore: STScI)
Jenkins, E. B. 2002, ApJ, 580, 938
Judge, P. G., & Carpenter, K. G. 1998, ApJ, 494, 828
Judge, P. G., & Stencel, R. E. 1991, ApJ, 371, 357
Karovska, M., Schlegel, E., Hack, W., Raymond, J. C., & Wood, B. E. 2005, ApJ, 623, L137

Kelch, W. L., Linsky, J. L., Basri, G. S., et al. 1978, ApJ, 220, 962
Kimble, R. A., Woodgate, B. E., Bowers, C. W., et al. 1998, ApJ, 492, L83
Lallement, R., Welsh, B. Y., Vergely, J. L., Crifo, F., & Sfeir, D. M., 2003, A&A, 411, 447
Lèbre, A., Aurière, M., Fabas, N., et al. 2014, A&A, 561, A85
Leenaarts, J., Pereira, T. M. D., Carlsson, M., Uitenbroek, H., & De Pontieu, B. 2013, ApJ, 772, 89
Linsky, J. L., & Avrett, E. H. 1970, PASP, 82, 169
Linsky, J. L., & Haisch, B. M. 1979, ApJ, 229, L27
Linsky, J. L., & Wood, B. E. 1996, ApJ, 463, 254
Mathioudakis, M., Fruscione, A., Drake, J. J., et al. 1995, A&A, 300, 775
Morton, D. C. 2003, ApJS, 149, 205
Mozurkewich, D., Armstrong, J. T., Hindsley, R. B., et al. 2003, AJ, 126, 2502
O'Gorman, E., Harper, G. M., Brown, A., Drake, S., & Richards, A. M. S. 2013, ApJ, 146, 98
Pauls, H. L., Zank, G. P., & Williams, L. L. 1995, J. Geophys. Res., 100, 21,595
Pérez Martínez, M. I., Schröder, K. -P., & Cuntz, M. 2011, MNRAS, 414, 418
Pourbaix, D., Tokovinin, A. A., Batten, A. H., et al. 2004, A&A, 424, 727
Rammacher, W., & Cuntz, M. 2003, ApJ, 594, L51
Redfield, S., & Linsky, J. L. 2002, ApJS, 139, 439
Redfield, S., & Linsky, J. L. 2004, ApJ, 602, 776
Redfield, S., & Linsky, J. L. 2008, ApJ, 673, 283
Reimers, D. 1975, in Problems in Stellar Atmospheres and Envelopes ed. B. Baschek, W. H. Kegel, & G. Traving (New York: Springer-Verlag), 229
Reimers, D. 1977, A&A, 57, 395
Reimers, D. 1982, A&A, 107, 292
Ribas, I., Guinan, E. F., Güdel, M., & Audard, M. 2005, ApJ, 622, 680
Robinson, R. D., Carpenter, K. G., & Brown, A. 1998, ApJ, 503, 396
Schmitt, J. H. M. M. 1997, A&A, 318, 215
Schrijver, C. J. 1987, A&A, 172, 111
Schröder, K. -P., Mittag, M., Pérez Martínez, M. I., Cuntz, M., & Schmitt, J. H. M. M. 2012, A&A, 540, A130
Sfeir, D. M., Lallement, R., Crifo, F., & Welsh, B. Y. 1999, A&A, 346, 785
Shu, F. H. 1992, The Physics of Astrophysics, Vol. II: Gas Dynamics (Mill Valley: University Science Books)
Snowden, S. L., Chiao, M., Collier, M. R., et al. 2014, ApJ, 791, L14
Snowden, S. L., Egger, R., Finkbeiner, D. P., Freyberg, M. J., & Plucinsky, P. P. 1998, ApJ, 493, 715
Stepien, K., & Ulmschneider, P. 1989, A&A, 216 ,139
Suzuki, T. K. 2007, ApJ, 659, 1592
Ulmschneider, P., Rammacher, W., Musielak, Z. E., & Kalkofen, W. 2005, ApJ, 631, L155
van Belle, G. T. 1999, PASP, 111, 1515
van Leeuwen, F. 2007, A&A, 474, 653
von Steiger, R., Wimmer-Schweingruber, R. F., Geiss, J., & Gloeckler, G. 1995, AdSpR, 15, 3
Wood, B. E., Harper, G. M., Müller, H. -R., Heerikhuisen, J., & Zank, G. P. 2007, ApJ, 655, 946
Wood, B. E., Izmodenov, V. V., Alexashov, D. B., Redfield, S., & Edelman, E. 2014a, ApJ, 780, 108
Wood, B. E., Müller, H. -R., Redfield, S., & Edelman, E. 2014b, ApJ, 781, L33
Wood, B. E., Müller, H. -R., & Witte, M. 2015, ApJ, 801, 62
Wood, B. E., Müller, H. -R., Zank, G. P., Linsky, J. L., & Redfield, S. 2005a, ApJ, 628, L143
Wood, B. E., Redfield, S., Linsky, J. L., Müller, H. -R., & Zank, G. P. 2005b, ApJS, 159, 118
Woodgate, B. E., Kimble, R. A., Bowers, C. W., et al. 1998, PASP, 110, 1183